1 Samples correlation for different C

All figures for $N = 100$, $\langle z \rangle = 4$, $T = 1.0$, $p = 0.50$.

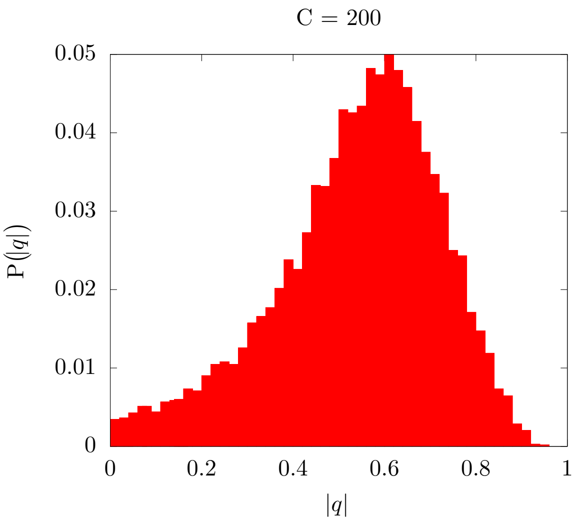

Figure 1.1

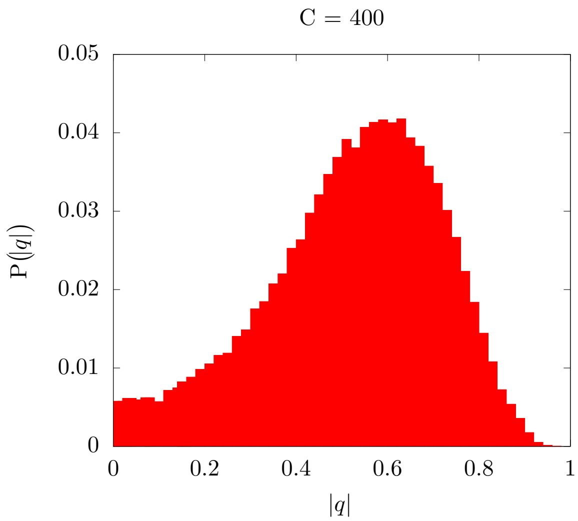

Figure 1.2

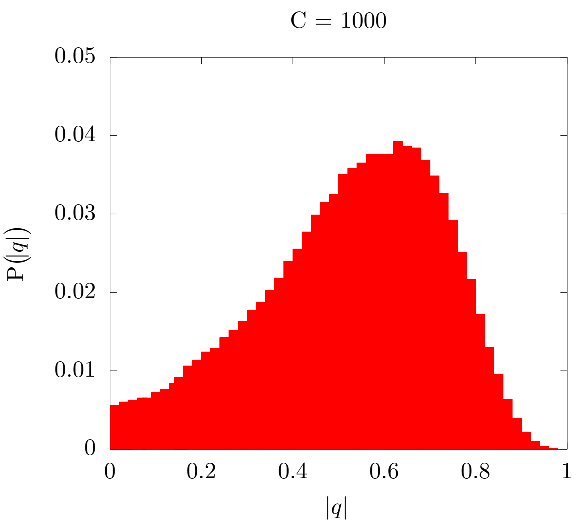

Figure 1.3

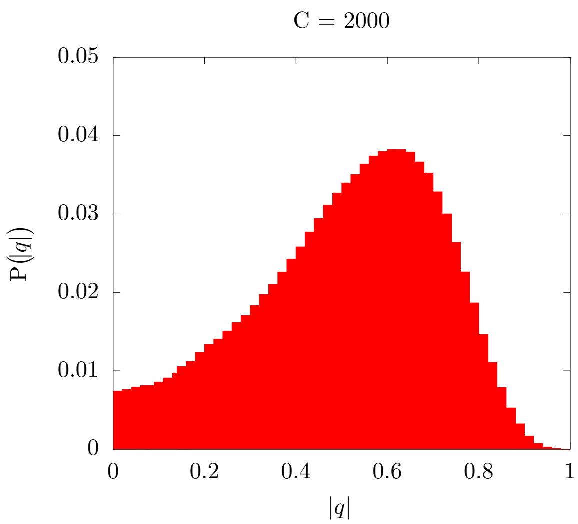

Figure 1.4

2 PL performance for different C

All figures for $N = 100$, $\langle z \rangle = 4$, $T = 1.0$, $p = 0.50$, $N_{\mathrm{g}} = 100$, $\tau = 2000$, $T_{\mathrm{F}}^{\mathrm{ini}} = 2.0$

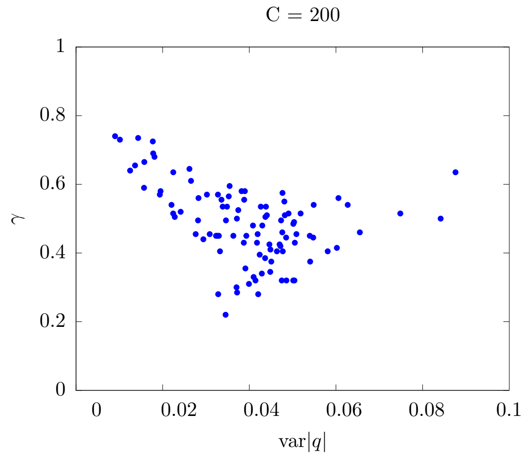

Figure 2.1

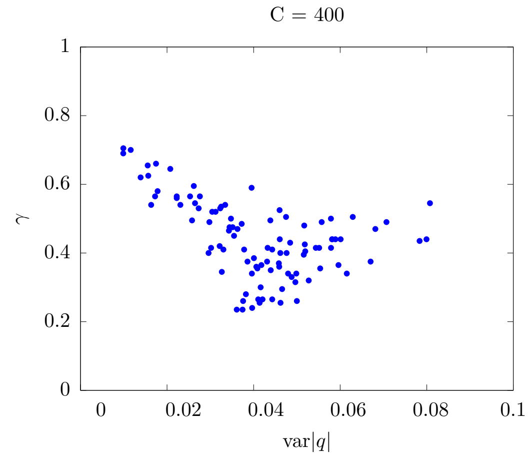

Figure 2.2

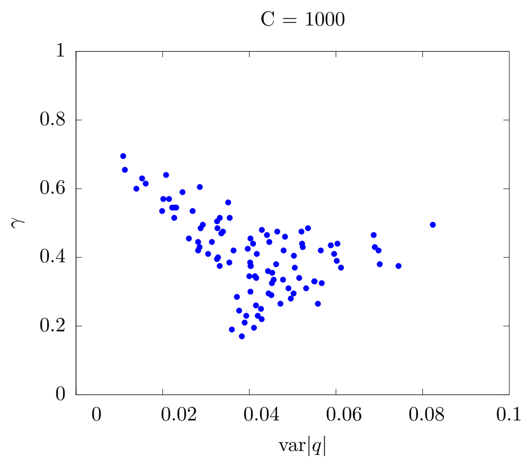

Figure 2.3

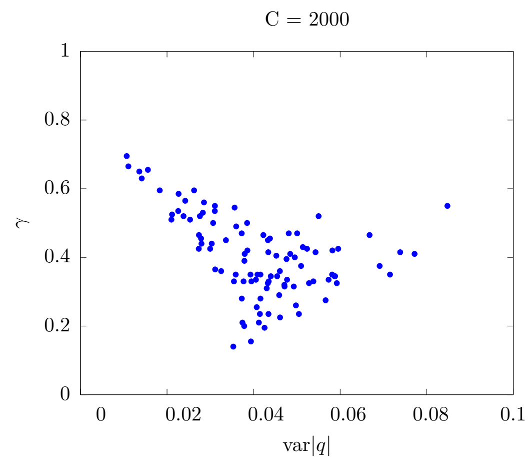

Figure 2.4

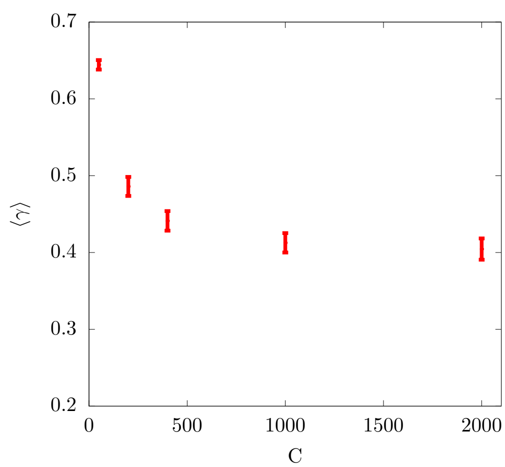

Figure 2.5: Dependency between average γ and the number of samples C.

3 PL performance for different τ

All figures for $N = 100$, $\langle z \rangle = 4$, $T = 1.0$, $p = 0.50$, $N_{\mathrm{g}} = 100$, C $= 400$, $T_{\mathrm{F}}^{\mathrm{ini}} = 0.04$.

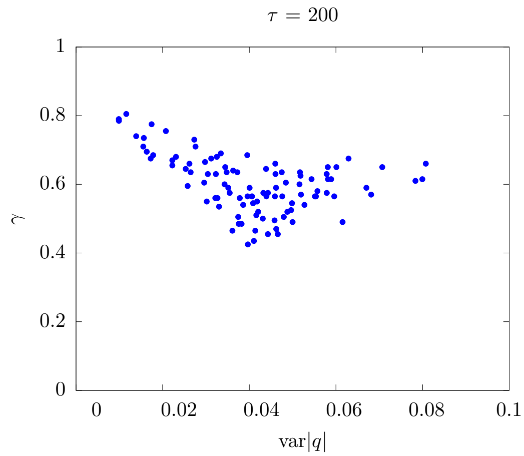

Figure 3.1

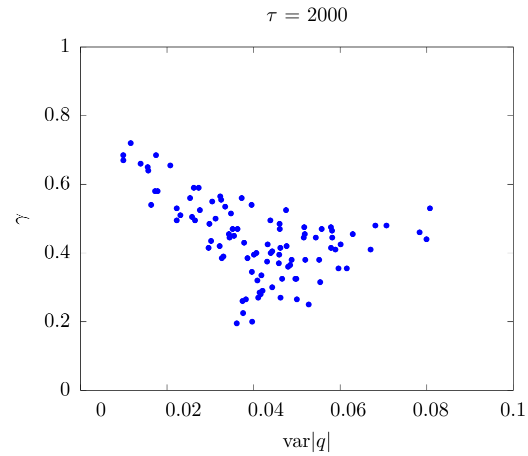

Figure 3.2

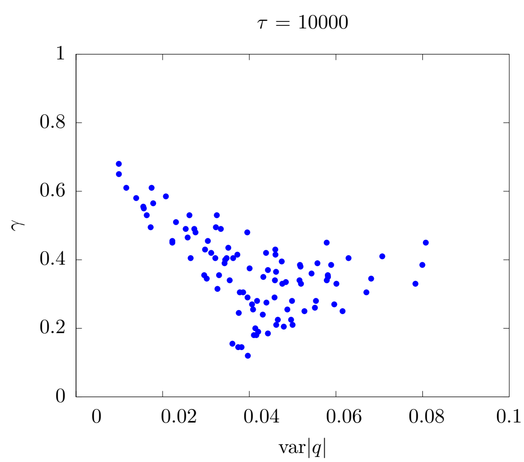

Figure 3.3

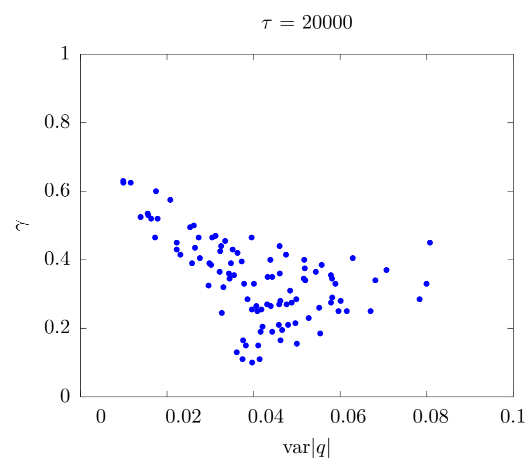

Figure 3.4

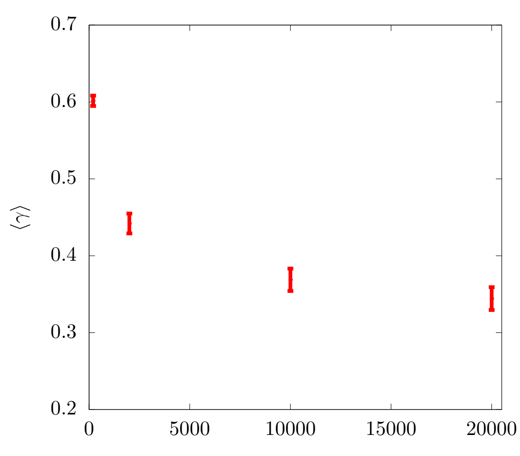

Figure 3.5: Dependency between average γ and the total number of Monte-Carlo steps τ.

4 Initial Fictitious Temperature effect on the PL performance

All figures for $N = 100$, $\langle z \rangle = 4$, $T = 1.0$, $p = 0.50$, $N_{\mathrm{g}} = 100$, $\mathrm{C} = 400$, $\tau = 1000$.

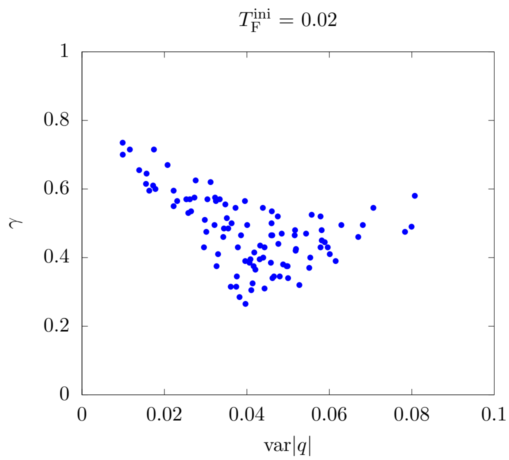

Figure 4.1

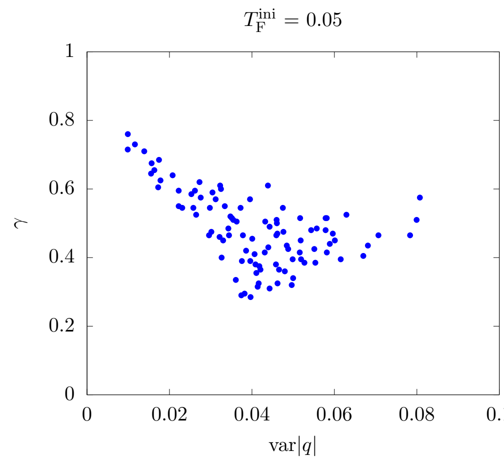

Figure 4.2

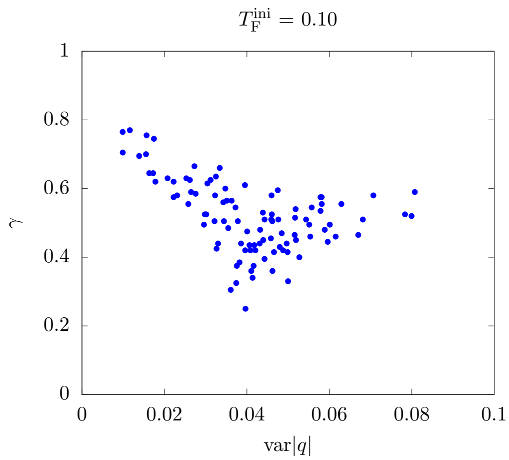

Figure 4.3

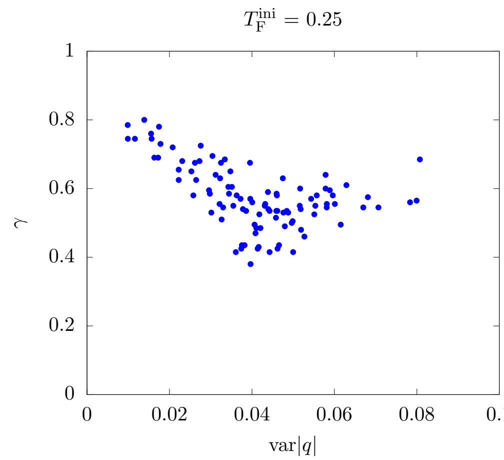

Figure 4.4

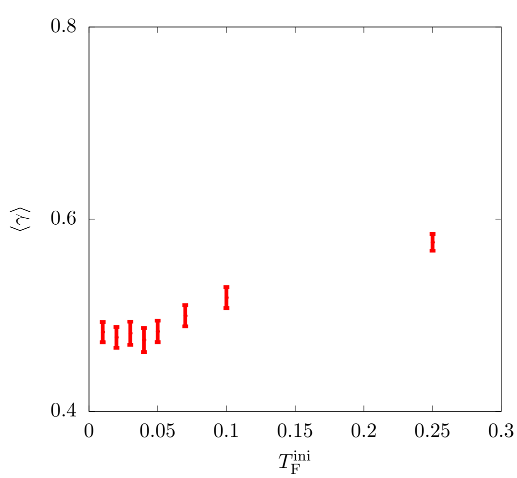

Figure 4.5: Dependency between average γ and the initial fictitious temperature of the simulated annealing.

5 Sample correlation distribution for all graphs with same p.

All figures for $N = 100$, $\langle z \rangle = 4$, $T = 1.0$, $N_{\rm g} = 100$, $\mathrm{C} = 1000$. Notice the vertical range difference for higher p values.

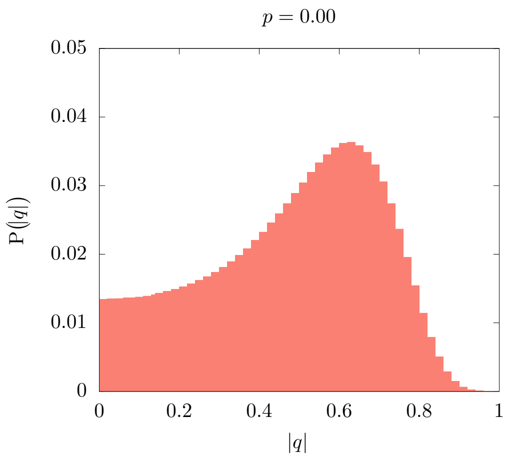

Figure 5.1

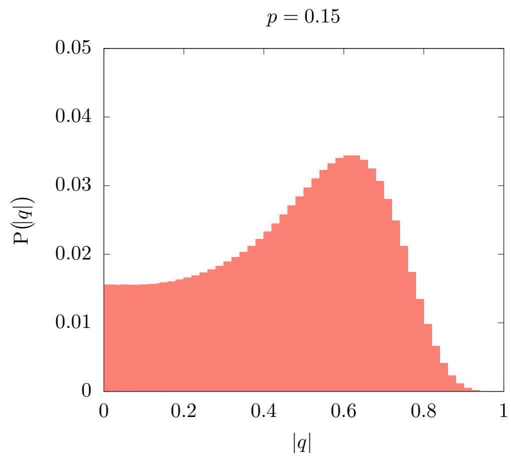

Figure 5.2

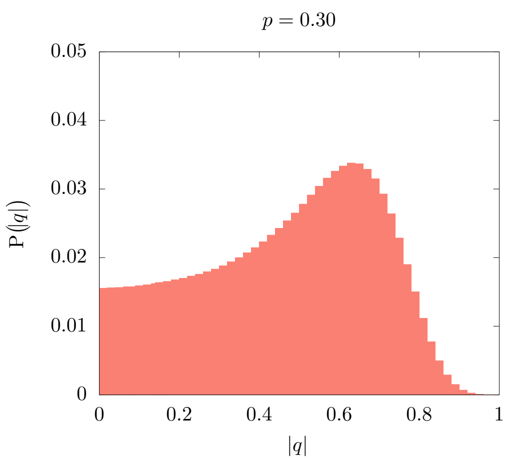

Figure 5.3

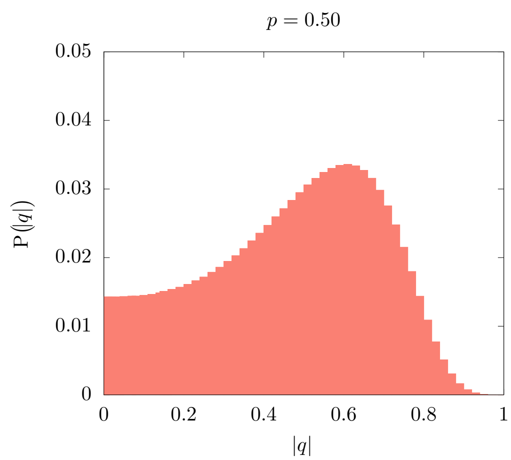

Figure 5.4

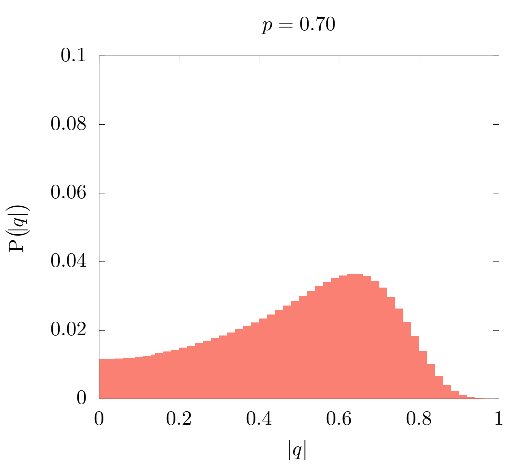

Figure 5.5

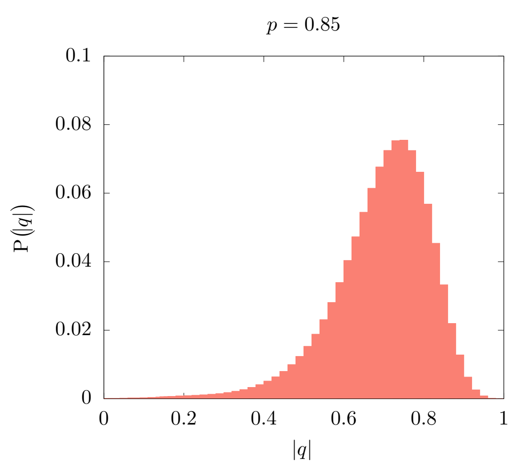

Figure 5.6

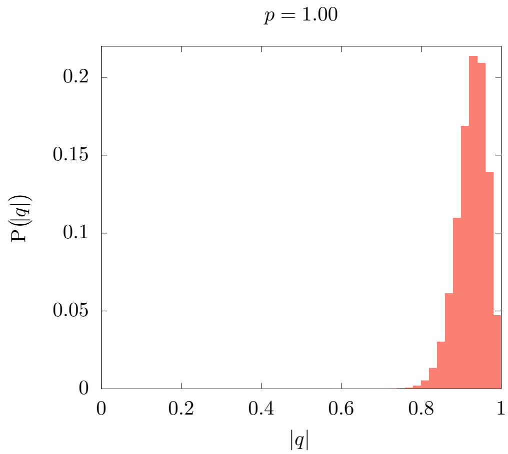

Figure 5.7

6 Sample correlation distribution for extreme PL performance graphs.

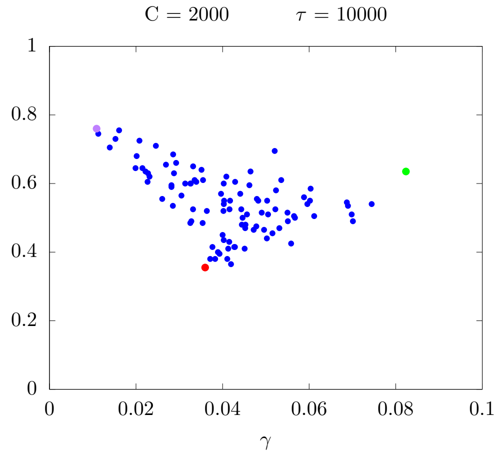

Figure 6.1: $N = 100$, $\langle z \rangle = 4$, $T = 1.0$, $p = 0.50$, $N_{\mathrm{g}} = 100$, $T_{\mathrm{F}}^{\mathrm{ini}} = 2.0$.

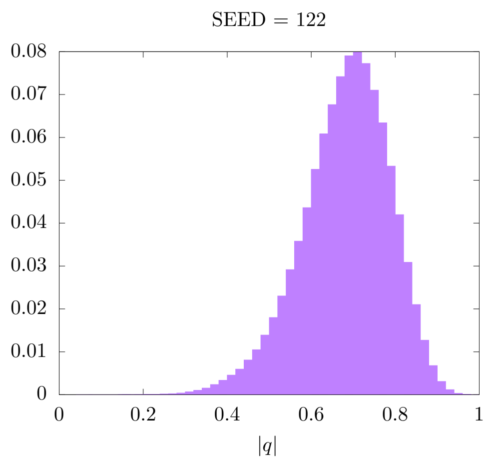

Figure 6.2: SEED with less var $|q|$ in Figure 6.1

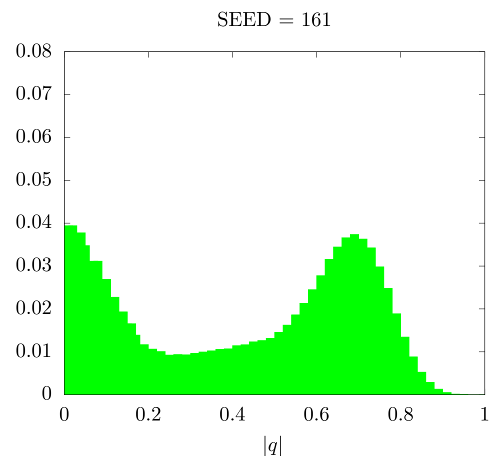

Figure 6.3: SEED with most var $|q|$ in Figure 6.1

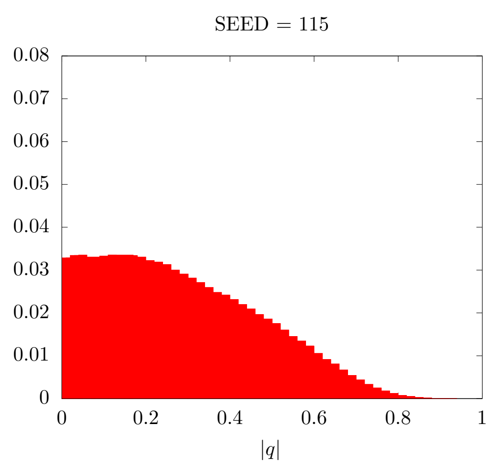

Figure 6.4: SEED with less γ in Figure 6.1

7 PL performance for C = 400, τ = 2000

All figures for $N = 100$, $\langle z \rangle = 4$, $T = 1.0$, $N_{\mathrm{g}} = 100$, $T_{\mathrm{F}}^{\mathrm{ini}} = 0.04$.

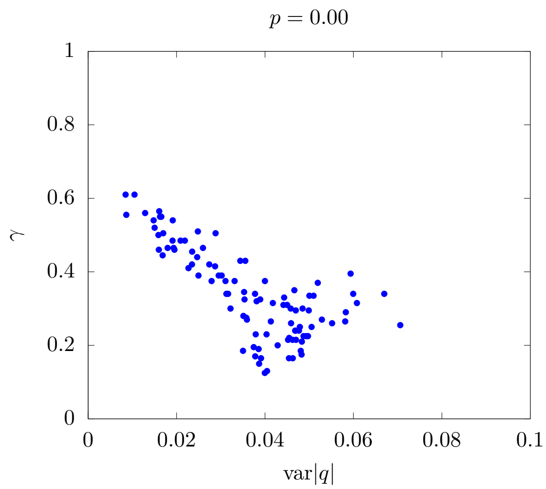

Figure 7.1

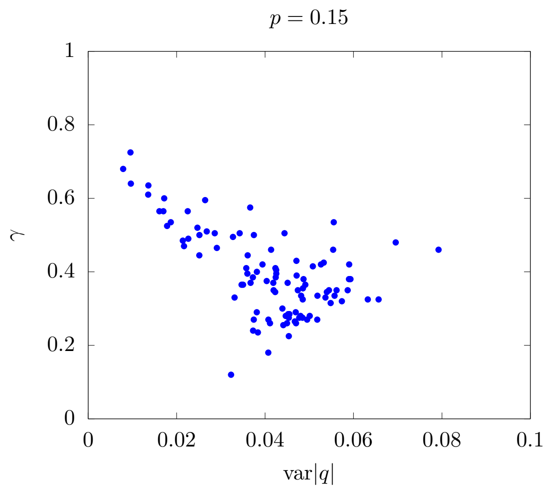

Figure 7.2

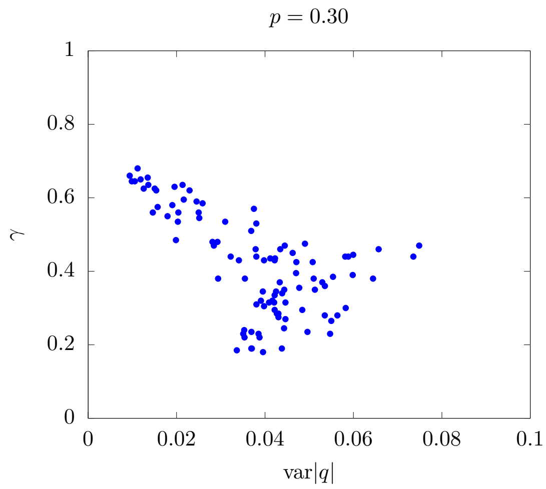

Figure 7.3

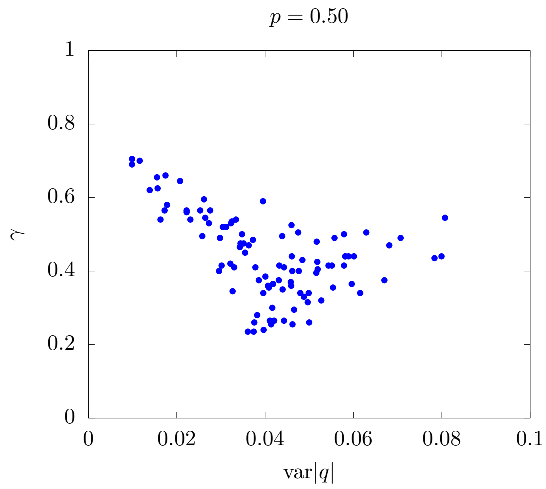

Figure 7.4

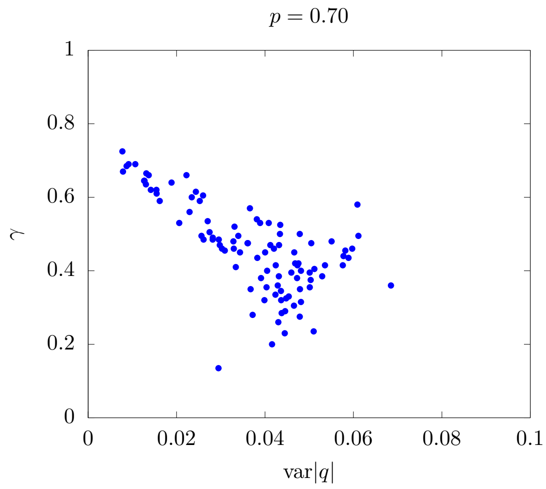

Figure 7.5

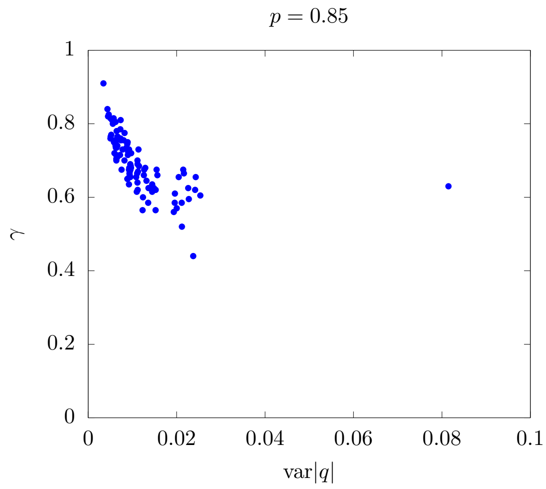

Figure 7.6

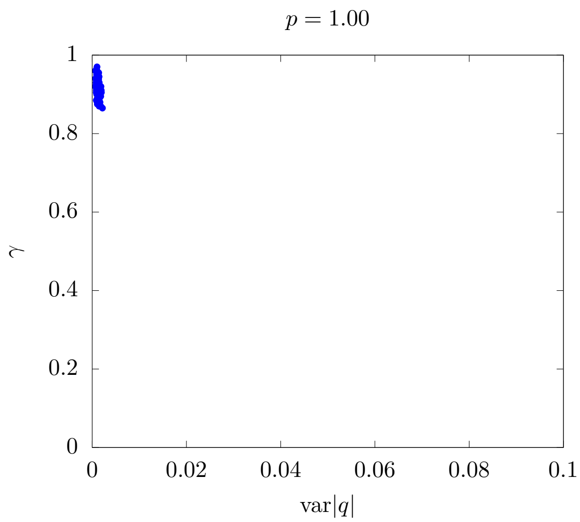

Figure 7.7

8 PL performance for different fictitious temperature reduction rhythms.

All figures for $N = 100$, $\langle z \rangle = 4$, $T = 1.0$, $N_{\mathrm{g}} = 100$, $T_{\mathrm{F}}^{\mathrm{ini}} = 0.04$, $\mathrm{C} = 400$, $\tau = 2000$.
($t \equiv$ current Monte-Carlo step)

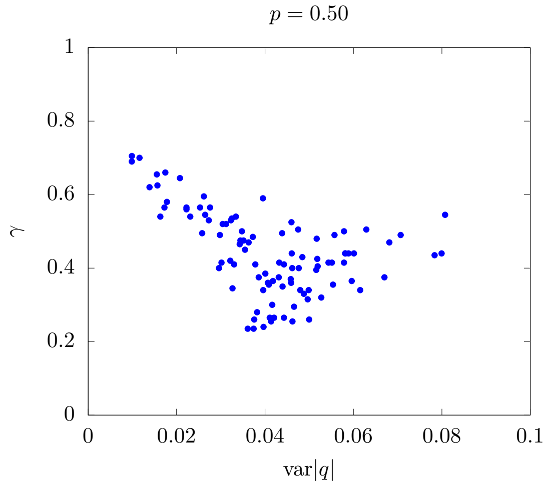

Figure 8.1: $T_{\mathrm{F}}(t) = T_{\mathrm{F}}^{\mathrm{ini}} \left(1 - \frac{t}{\tau}\right)$

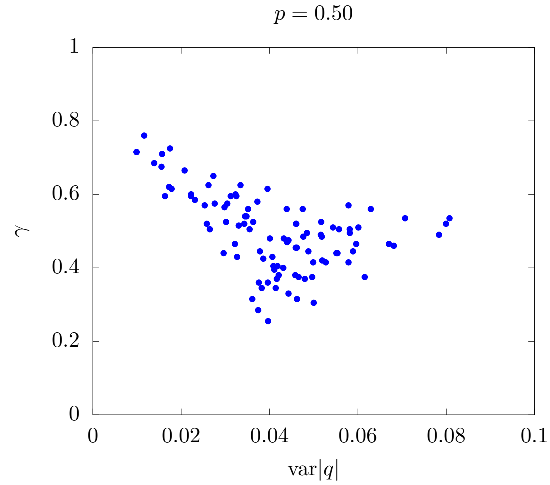

Figure 8.2: $T_{\mathrm{F}}(t) = \frac{T_{\mathrm{F}}^{\mathrm{ini}}}{\ln t} \left(1 - \frac{t}{\tau}\right)$

All the figures in this document are done with the Figure 8.1 equation.

9 Consistency of the PL performance

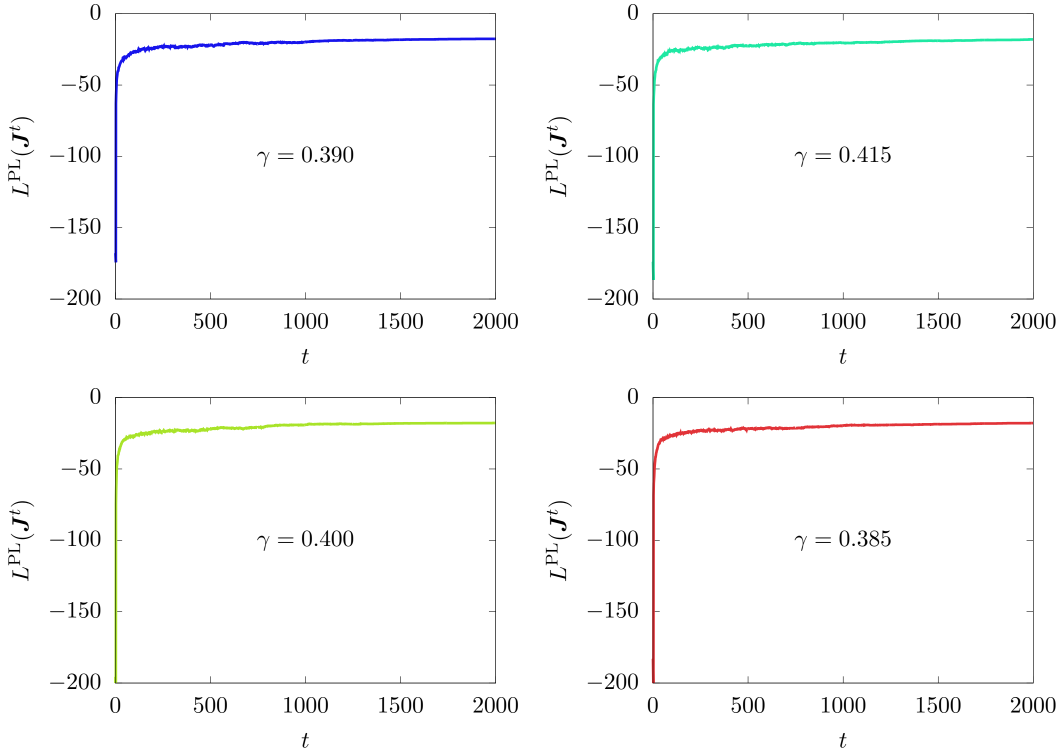

Figure 9.1: PL evolution in 4 different Monte-Carlo simulations for the SEED = 100 with $N = 100$, $\langle z \rangle = 4$, $p = 0.50$, $p = 1.0$, $T_{\mathrm{F}}^{\mathrm{ini}} = 0.04$, C = 400, $\tau = 2000$.

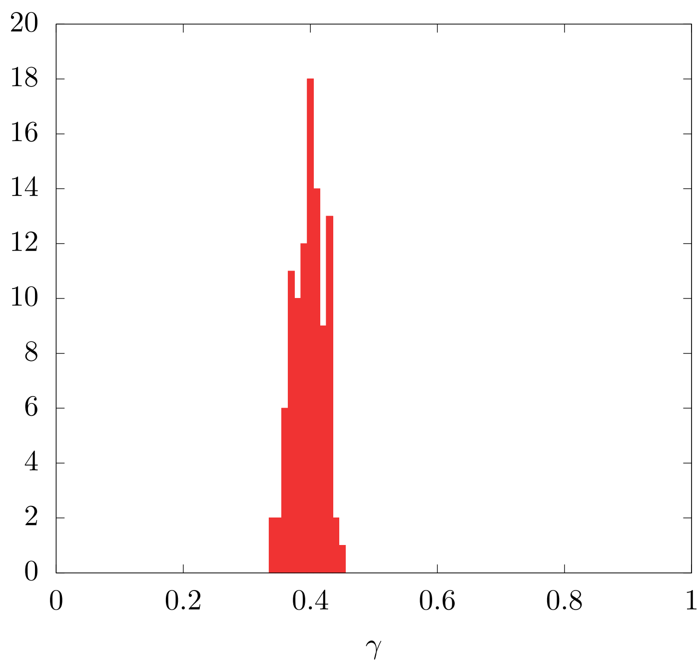

Figure 9.2: Gamma distribution in 100 different Monte-Carlo simulations for the SEED = 100 with $N = 100$, $\langle z \rangle = 4$, $p = 0.50$, $T = 1.0$, $T_{\mathrm{F}}^{\mathrm{ini}} = 0.04$, C = 400, $\tau = 2000$.

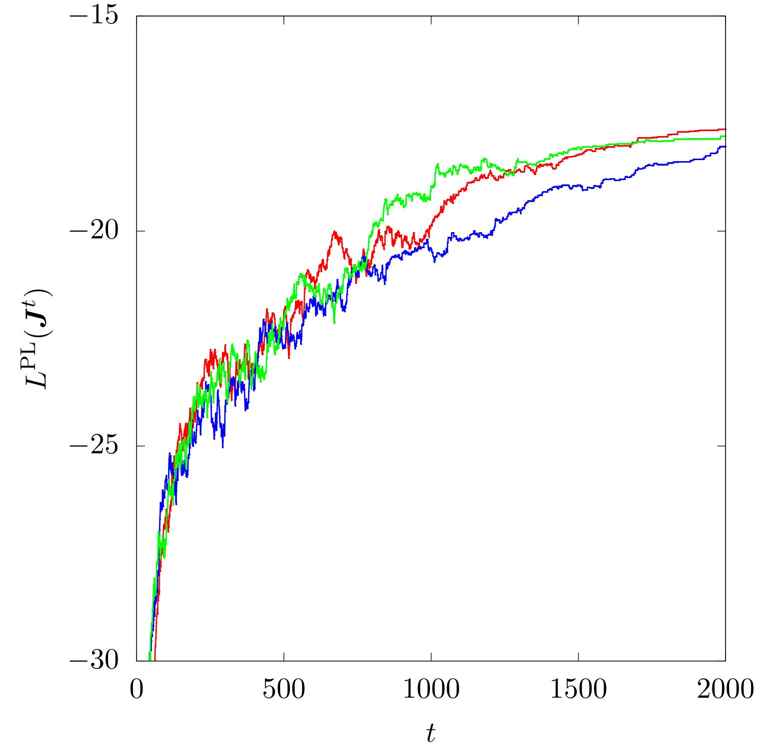

Figure 9.3: PL evolution in 3 different Monte-Carlo simulations zoomed in for the SEED = 100 with $N = 100$, $\langle z \rangle = 4$, $p = 0.50$, $T = 1.0$, $T_{\mathrm{F}}^{\mathrm{ini}} = 0.04$, C = 400, $\tau = 2000$.

10 Samples correlation for different T

All figures for $N = 100$, $C = 400$, $\langle z \rangle = 4$, $N_{\mathrm{g}} = 100$.

$p = 0.00$ $p = 0.15$ $p = 0.30$ $p = 0.50$ $p = 0.70$ $p = 0.85$ $p = 1.00$

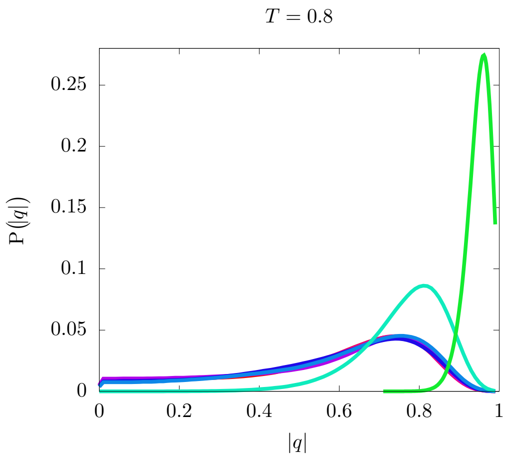

Figure 10.1

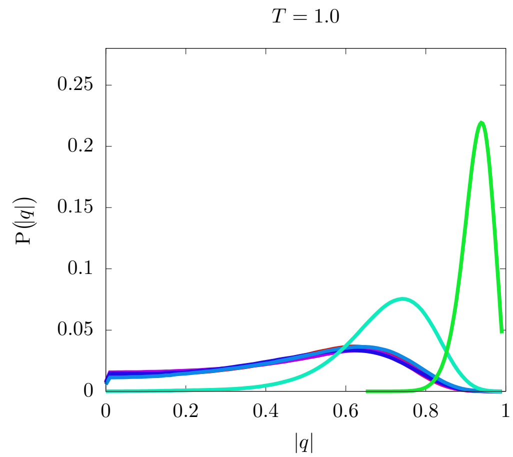

Figure 10.2

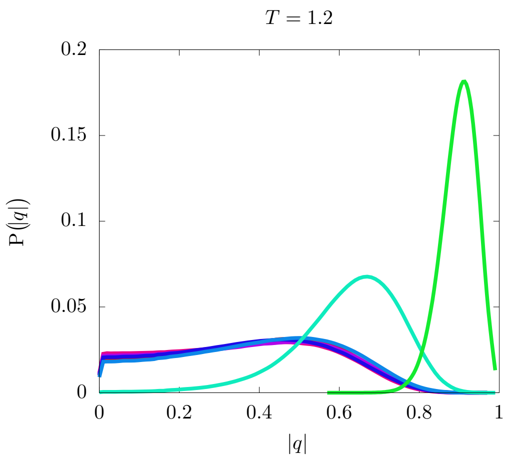

Figure 10.3

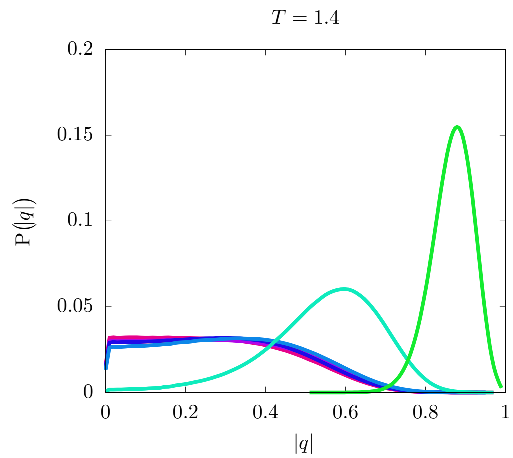

Figure 10.4

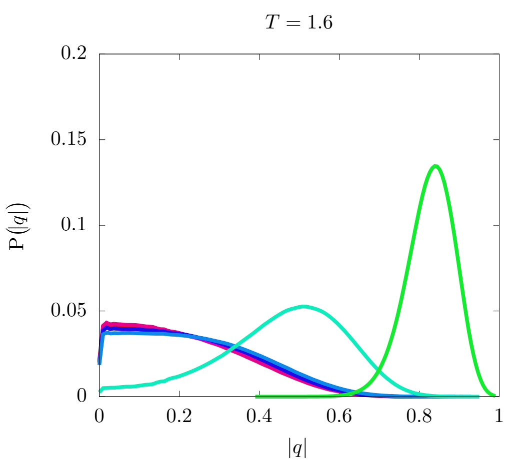

Figure 10.5

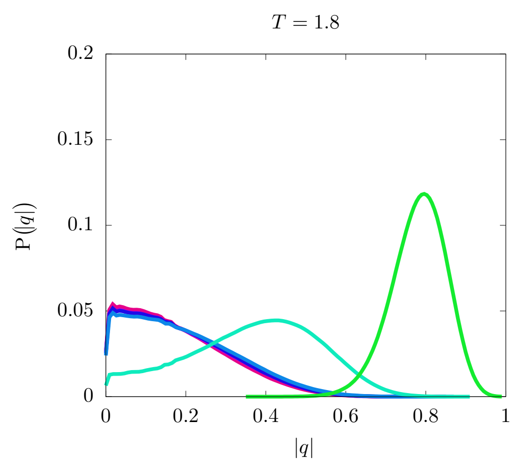

Figure 10.6

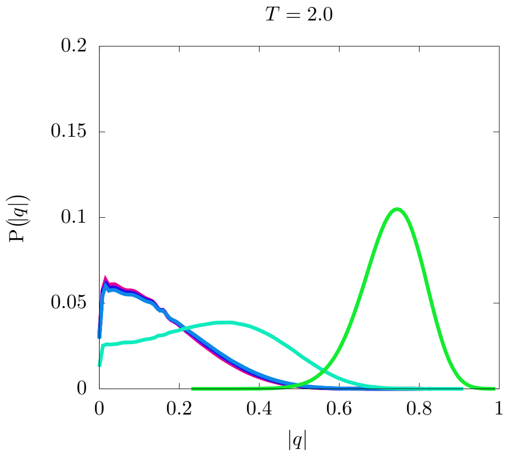

Figure 10.7

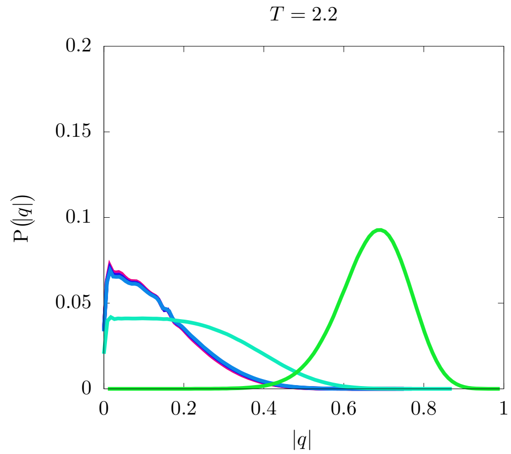

Figure 10.8

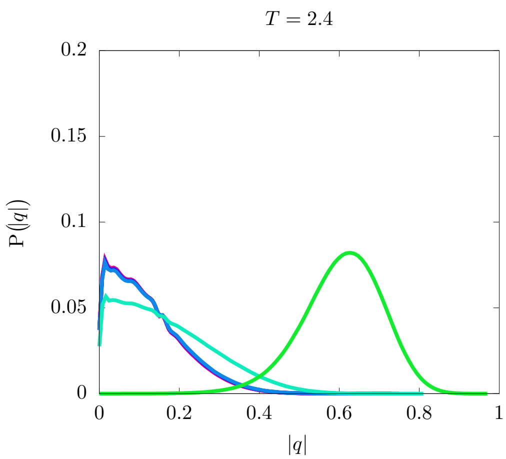

Figure 10.9

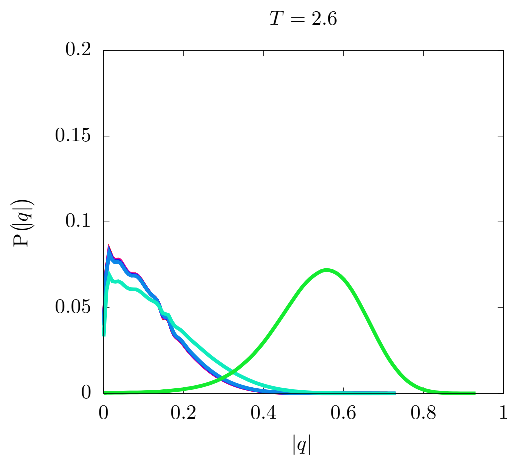

Figure 10.10

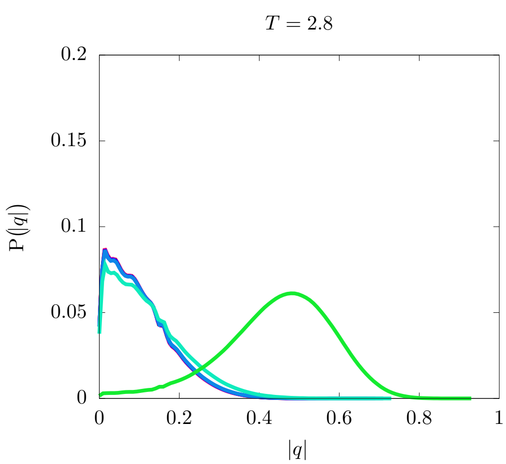

Figure 10.11

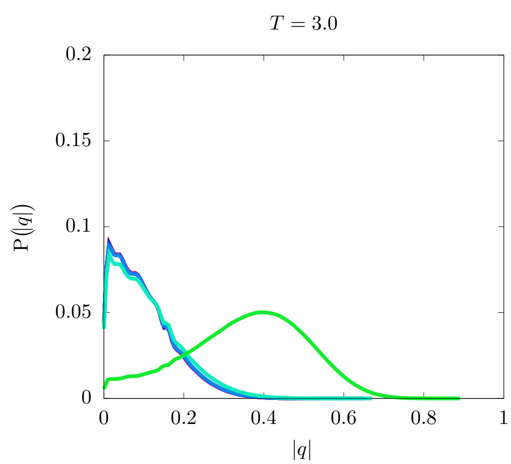

Figure 10.12

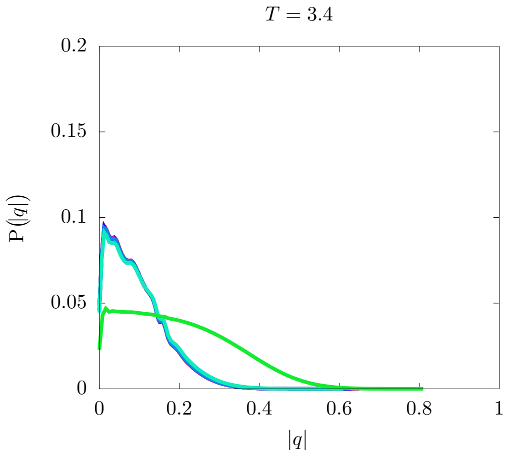

Figure 10.13

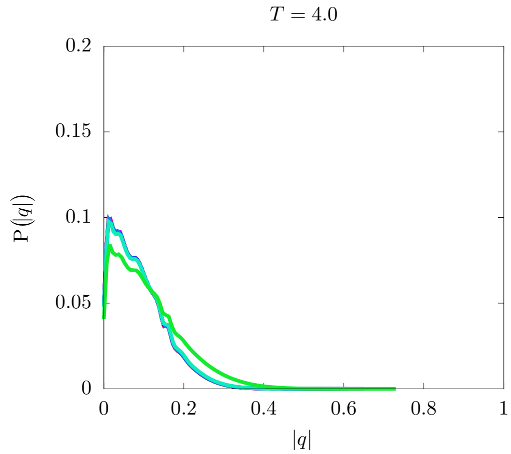

Figure 10.14

11 PL performance for different T

Considering $N = 100$, $\langle z \rangle = 4$, $N_{\mathrm{g}} = 100$, $\mathrm{C} = 400$, $\tau = 2000$ and $T_{\mathrm{F}}^{\mathrm{ini}} = -\frac{1}{3} \ln \left[\frac{1}{2} \left(1 + \tanh \frac{1}{T} \right) \right]$

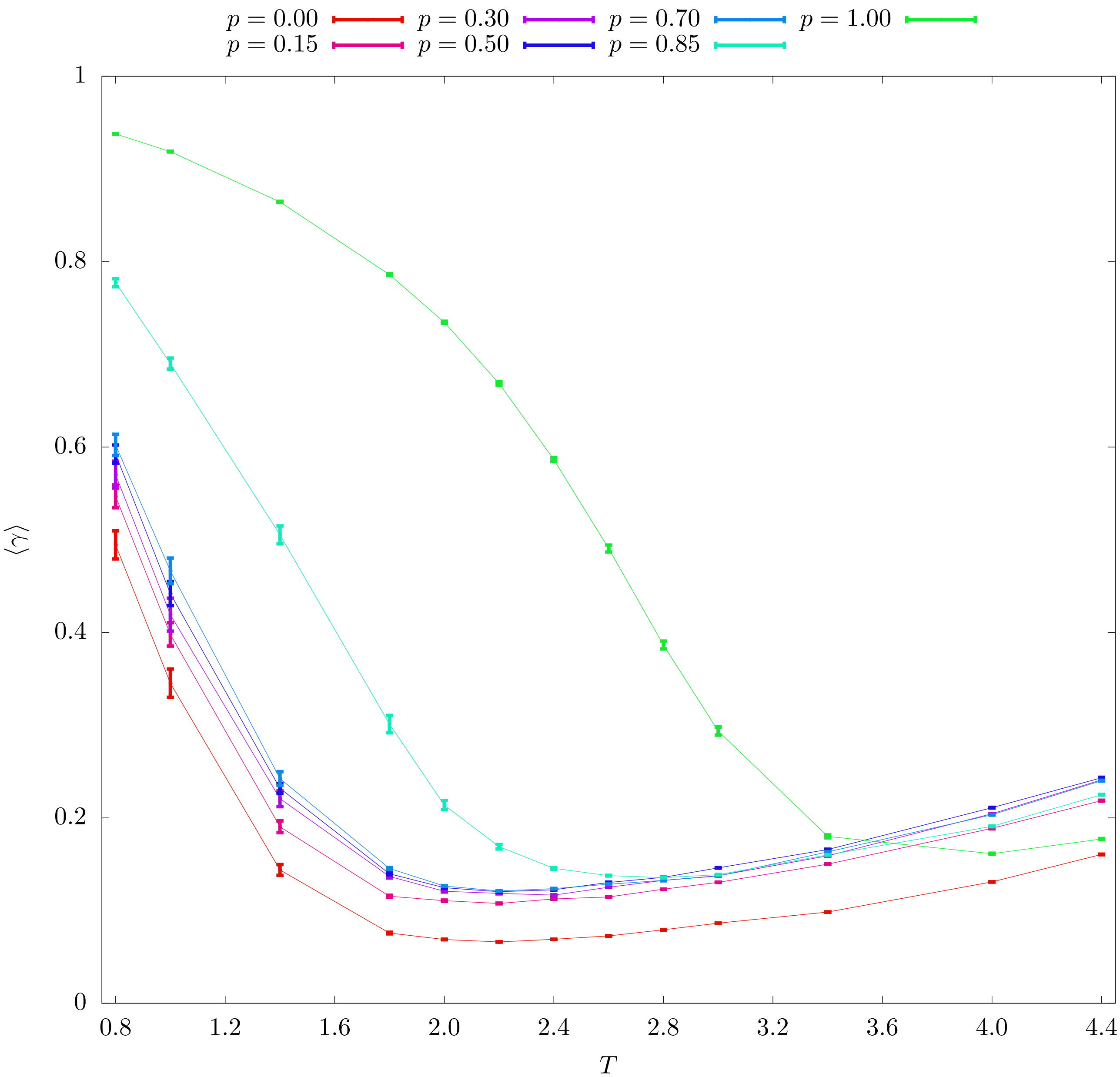

Figure 11.1: PL performance in relation to T for different p.

12 Phase Diagram

In [1] the following equations are obtained, for random ferromagnetic and anti-ferromagnetic interactions of equal strength $\pm J$ and a average connectivity $\langle z\rangle$,

$$\langle \tanh^2(J/T_{\mathrm{SG}})\rangle_J = \frac{1}{\langle z\rangle} \qquad \langle \tanh(J/T_{\mathrm{FM}})\rangle_J = \frac{1}{\langle z\rangle} \tag{12.1}$$

So since the pairwise distribution in this project system is

$$P(J_{ij}) = p\cdot\delta(J_{ij}-1) + (1-p)\cdot\delta(J_{ij}+1) \tag{12.2}$$

and $\langle z\rangle = 4$, the relation between the different phase temperature transition and p are

$$T_{\mathrm{SG}}^{-1} = \operatorname{arctanh}\frac{1}{2} \qquad T_{\mathrm{FM}}^{-1} = \operatorname{arctanh}\frac{1}{4(2p-1)} \tag{12.3}$$

According to [2] the SG-FM transition at $T = 0$ is around $p = 0.73$, with a mixed phase up to $p = 0.8$, with this and knowing from [1] that this phases are split vertically near the multi-critical point, a full phase diagram can be drawn:

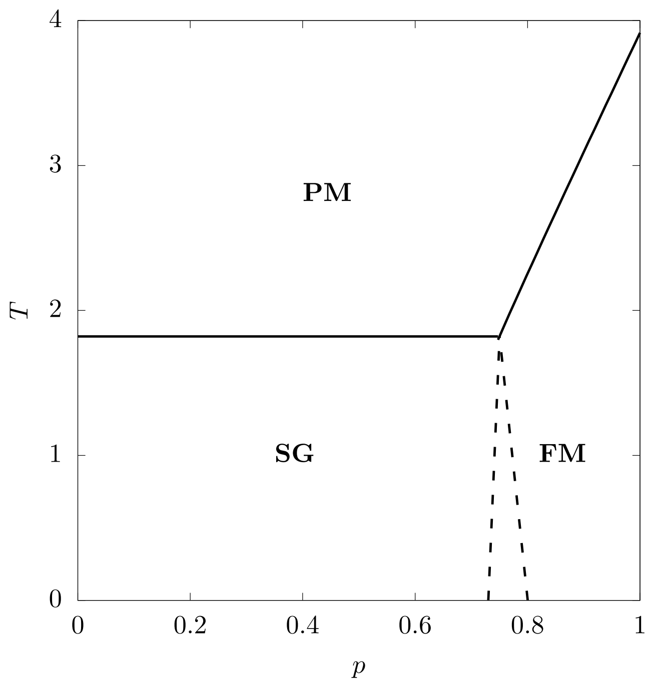

Figure 12.1

References

[1] L.Viana and A.J. Bray *Phase diagrams for dilute spin glasses*, (J. Phys. C: Solid State Phys. 18 3037 (1985)).

[2] M.O. Hase *Spin-glass behaviour on random lattices*, (J. Stat. Mech. (2012)).

13 PL performance and average magnetization per sample relation

All figures for $N = 100$, $\langle z \rangle = 4$, $T = 1.0$, $N_{\mathrm{g}} = 100$, $T_{\mathrm{F}}^{\mathrm{ini}} = 0.04$.

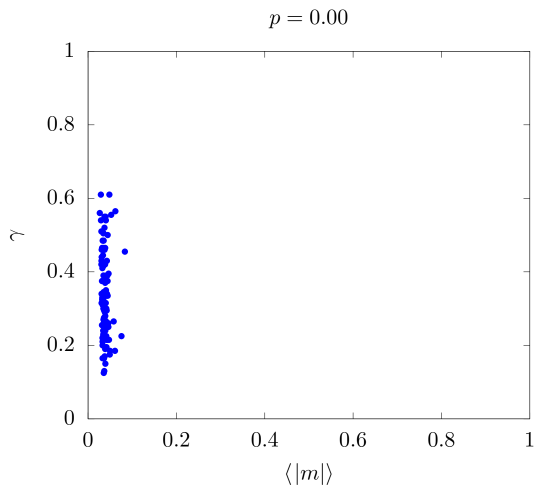

Figure 13.1

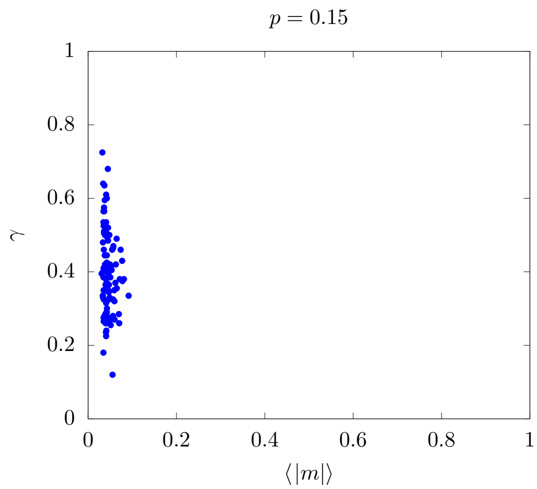

Figure 13.2

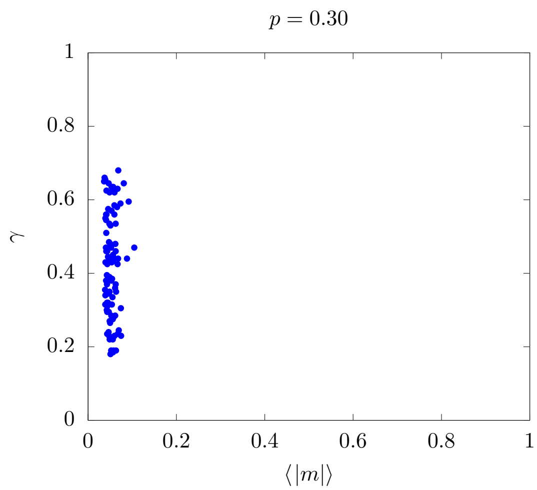

Figure 13.3

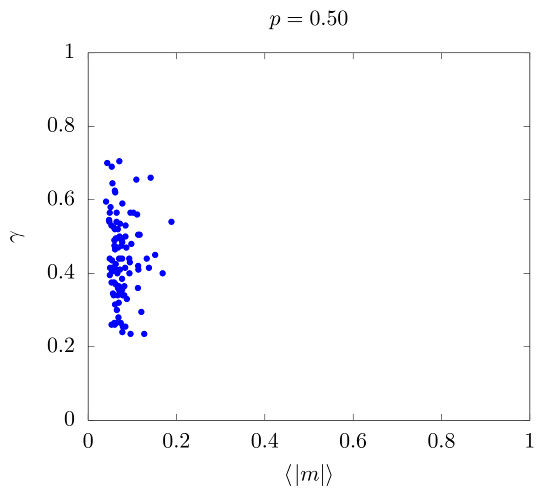

Figure 13.4

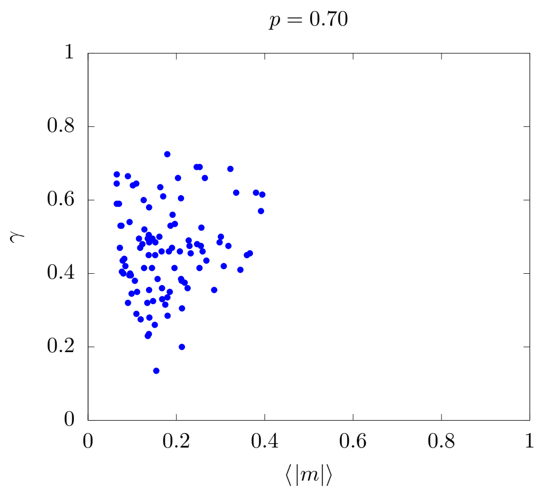

Figure 13.5

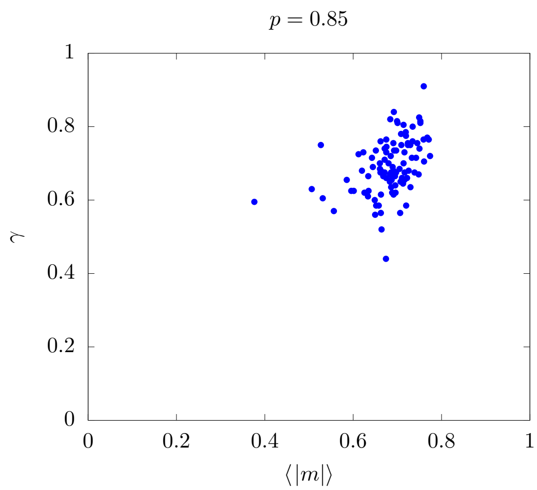

Figure 13.6

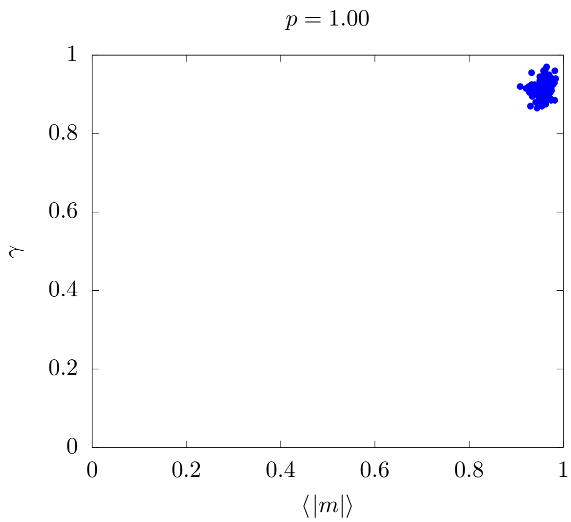

Figure 13.7

14 Average Sample Energy gamma dependency for C = 400, τ = 1000

All figures for $N = 100$, $\langle z \rangle = 4$, $T = 1.0$, $N_\mathrm{g} = 100$, $T_\mathrm{F}^\mathrm{ini} = 2.0$.

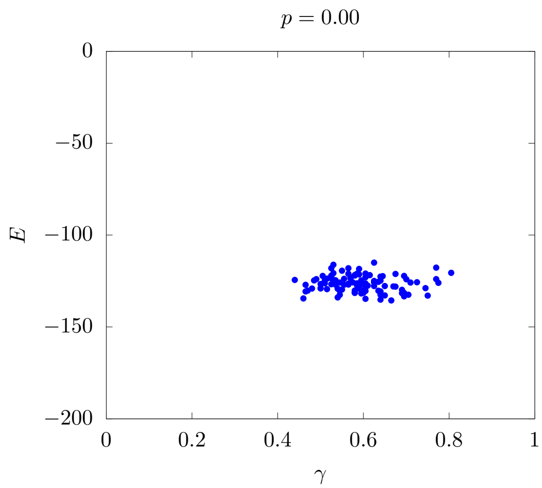

Figure 14.1

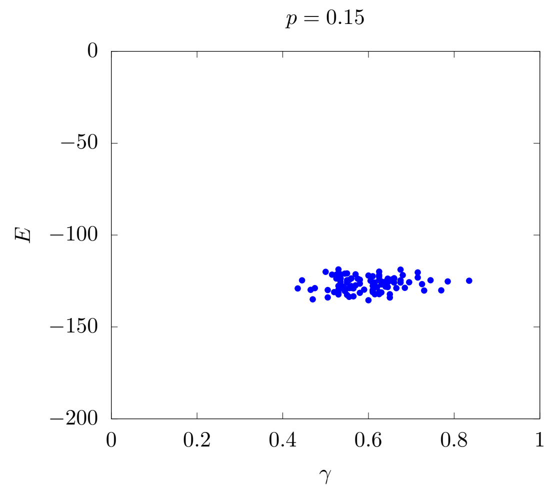

Figure 14.2

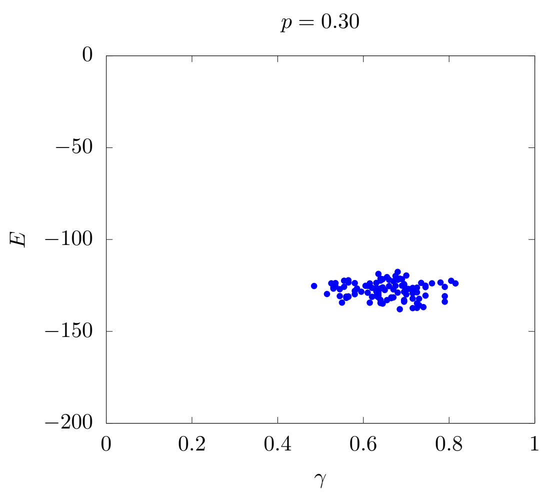

Figure 14.3

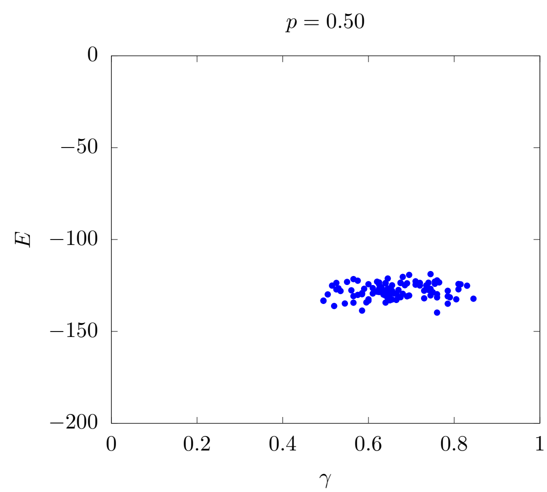

Figure 14.4

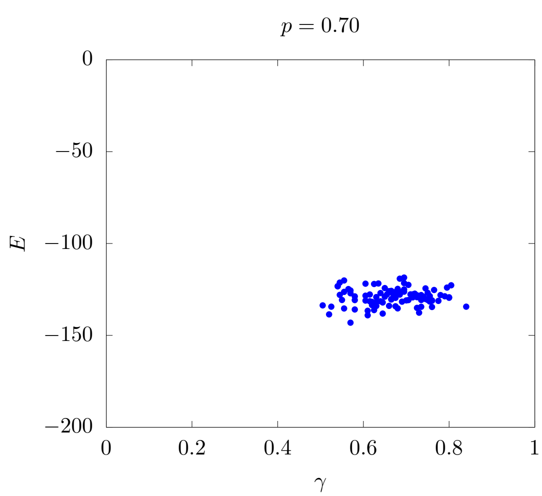

Figure 14.5

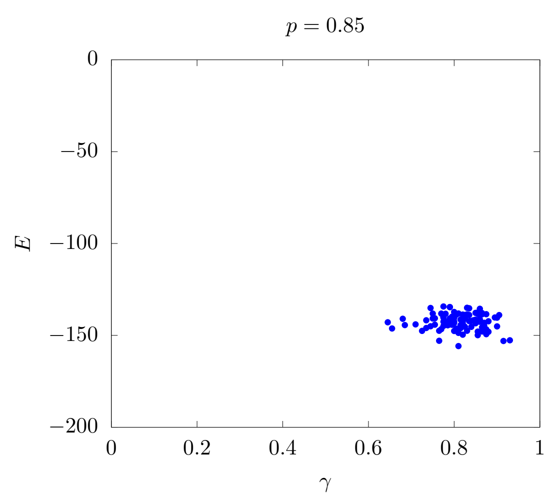

Figure 14.6

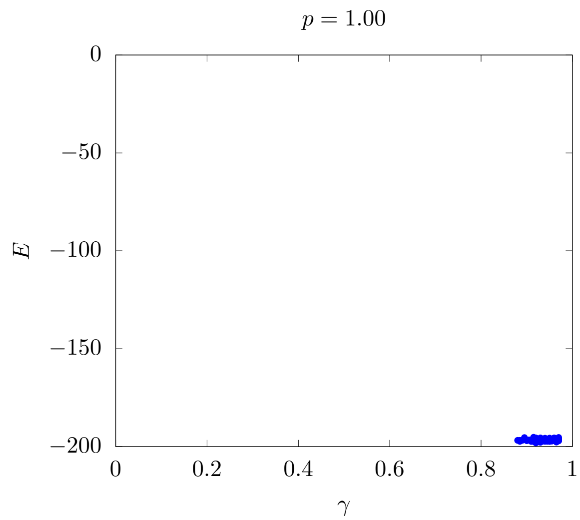

Figure 14.7